RSC Advances

PAPER

View Article Online
View Journal | View Issue

Cite this: *RSC Adv.*, 2025, **15**, 38986

Dual-functional molecule 3c targeting CYP24A1-mediated 25-hydroxyvitamin D metabolism and microbial biofilms overcomes mixed vaginal infections

Xiaojie Wang, * Ye Liu, Chuan Sun, Hemin Li and Jing Xu

In the context of clinical treatment for mixed vaginal infections, which pose dual challenges of biofilm resistance and immune microenvironment imbalance, this study synthesized 12 "triazole–Schiff base" hybrid compounds using previously reported synthetic routes. This design was guided by the core mechanism in which CYP24A1 enzyme overexpression in the vitamin D–vitamin D receptor immunoregulatory pathway leads to degradation of active vitamin D. Among them, compound **3c** exhibited excellent broad-spectrum antibacterial and antifungal activity (MIC = 16 μg mL^{-1}), low cytotoxicity, and significant inhibition and eradication of *Candida albicans* biofilms. Mechanistic studies revealed that the compound possesses both membrane-targeting disruptive effects and CYP24A1 inhibitory activity. At the enzymatic level, compound **3c** achieved 32% inhibition of CYP24A1 at 100 μM. In cellular models, it did not affect basal CYP24A1 mRNA expression at 10^{-7} M, but when combined with $1,25(OH)_2D_3$, it up-regulated CYP24A1 mRNA levels approximately twofold. Further LC-MS/MS analysis confirmed that the addition of 10^{-7} M of compound **3c** significantly slowed the metabolic clearance of $1,25(OH)_2D_3$ in HEK293T cells, maintaining an average concentration of 495 pM after 24 h. In summary, compound **3c** employs a multi-target synergistic mechanism of "direct antimicrobial activity–immunomodulation–biofilm penetration" to effectively overcome biofilm-mediated resistance and improve the local immune microenvironment, thus offering a promising lead compound with clinical translational potential for addressing the therapeutic challenges in mixed infections.

Received 9th September 2025
Accepted 2nd October 2025

DOI: 10.1039/d5ra06803g

rsc.li/rsc-advances

1. Introduction

In the field of female reproductive tract health, aberrant symbiotic interactions between vaginal bacteria and fungi are driving an emerging clinical crisis.[1,2] Mixed infections, primarily represented by bacterial vaginosis (BV) and vulvovaginal candidiasis (VVC), account for up to 34% of cases, with their core pathological manifestation being the formation of resilient biofilm consortia by *Candida albicans* and other fungal species.[3,4] Bacterially derived sialidase disrupts the mucosal barrier, creating pathways for fungal hyphal invasion, while *Candida*-secreted lysophospholipase promotes bacterial biofilm maturation. This synergy enables both pathogens to collectively resist host immune clearance and enhance antibiotic tolerance.[5,6] The current standard therapy, *i.e.*, sequential administration of metronidazole and fluconazole, faces substantial challenges: rising azole resistance in *Candida* species and persistently high recurrence rates of mixed infections.[7,8] The underlying issue is the fact that conventional drugs only transiently suppress planktonic pathogens, remain ineffective against biofilm-embedded infections, and completely overlook the compromised mucosal immunity as a core pathological basis.[9,10] Therefore, developing multi-target inhibitors capable of simultaneously penetrating biofilm barriers, precisely eradicating pathogenic networks, and activating local immune defenses has become a strategic imperative to overcome the current therapeutic dilemma.

The central role of the vitamin D metabolic pathway in regulating immunity against reproductive tract infections offers a novel perspective for intervention.[11] As a natural immunomodulator, active vitamin D ($1,25-(OH)_2D_3$) binds to the vitamin D receptor (VDR) in vaginal epithelial cells and activates multiple defense mechanisms: it induces the expression of the antimicrobial peptide LL-37, which disrupts bacterial cell membranes and inhibits fungal β-glucan synthase; down-regulates the NF κB pathway, reducing pro-inflammatory cytokines such as IL-1β and TNF-α; and enhances the expression of the tight junction protein occludin to restore the physical barrier.[12–14] Vaginal infections trigger a local inflammatory response that leads to increased levels of pro-inflammatory cytokines such as TNF-α and IL-1β. These cytokines have been

The Second Hospital of Qinhuangdao, Gynecology, Qinhuangdao, 066000, China. E-mail: 19316050169@163.com

shown to upregulate the expression of CYP24A1, thereby accelerating the degradation of active vitamin D.[15] Clinical studies have confirmed that the concentration of 1,25-$(OH)_2D_3$ in vaginal lavage fluids of patients with mixed infections is less than 30% of that in healthy individuals, creating a vicious cycle of "immune suppression → pathogen proliferation → enzymatic activation".[16,17] Although azole-based CYP24A1 inhibitors such as VID400 have entered clinical trials, their hepatotoxicity and lack of antifungal activity (MIC > 128 μg mL^{-1} against *Candida albicans*) limit their therapeutic potential.[18,19]

To address the aforementioned challenges, this study proposes a "triazole–Schiff base synergistic pharmacophore" design strategy. The triazole ring is a recognized antifungal pharmacophore, as exemplified by fluconazole, and possesses potent antimicrobial activity. Schiff bases exhibit a broad spectrum of biological activities, including antibacterial, antibiofilm, and metal-chelating capabilities. Our hybridization strategy aims to amalgamate membrane-targeting effects (potentially associated with the Schiff base) and enzyme inhibition (likely mediated by the triazole ring targeting CYP450 family enzymes) within a single molecule. This design is anticipated to yield synergistic or additive effects while potentially reducing the risk of resistance associated with azole monotherapy. Furthermore, the Schiff base moiety serves as an excellent pharmacophore linker, and its synthetic flexibility will facilitate future structural optimization of the lead compounds. Notably, Schiff bases have been demonstrated to possess broad-spectrum antimicrobial activity, particularly against BV-associated anaerobes such as *Gardnerella* and *Mobiluncus*, *via* mechanisms involving disruption of microbial membrane potential and interference with energy metabolism. Using the 1,2,4-triazole ring as the core structure should provide strong CYP24A1-binding capacity, while its amphiphilic nature may further confer membrane-targeting disruptive effects, as illustrated in Fig. 1A. This design offers a "targeted delivery" advantage, and the molecular hybridization of a triazole and Schiff base is expected to generate novel biological activities beyond those of single pharmacophores through synergistic effects. Its intrinsic antibacterial property, combined with host immune activation through CYP24A1 inhibition, indicates the potential of this compound series to achieve synergistic efficacy *via* a dual mechanism of "direct bactericidal action + indirect immune regulation", thereby opening a new paradigm for anti-infective drug design in the era of drug resistance.

2. Results and discussion

2.1 Chemical synthesis

Building upon previous studies,[20,21] this work synthesized 12 previously reported triazole–Schiff base CYP24A1 inhibitors (compounds **3a–3l**) *via* a two-step reaction. As illustrated in Fig. 1B, the synthesis started with aminoguanidine as the molecular scaffold. A triazole ring (3-amino-1,2,4-triazole) was introduced to enhance coordination with the heme iron of CYP24A1, while the dynamic nature of the Schiff base linkage was utilized to improve binding adaptability. In contrast to conventional Schiff base synthesis methods, all final products were obtained without the need for column chromatography purification; instead, they were washed with anhydrous ethanol and recrystallized. All compounds were fully characterized by ^{1}H NMR, ^{13}C NMR, mass spectrometry, and melting point determination, which were consistent with data reported in the literature. It is worth noting that the final products **3a–3l** exhibited limited solubility in deuterated DMSO, which may account for the relatively weak signals and/or elevated baseline noise observed in their ^{1}H and ^{13}C NMR spectra.

2.2 Determination of minimum inhibitory concentration

Based on the design concept of developing dual-functional agents targeting both bacterial pathogens and fungi in the vaginal microenvironment, while specifically inhibiting CYP24A1, Schiff base–triazole conjugates were synthesized, and

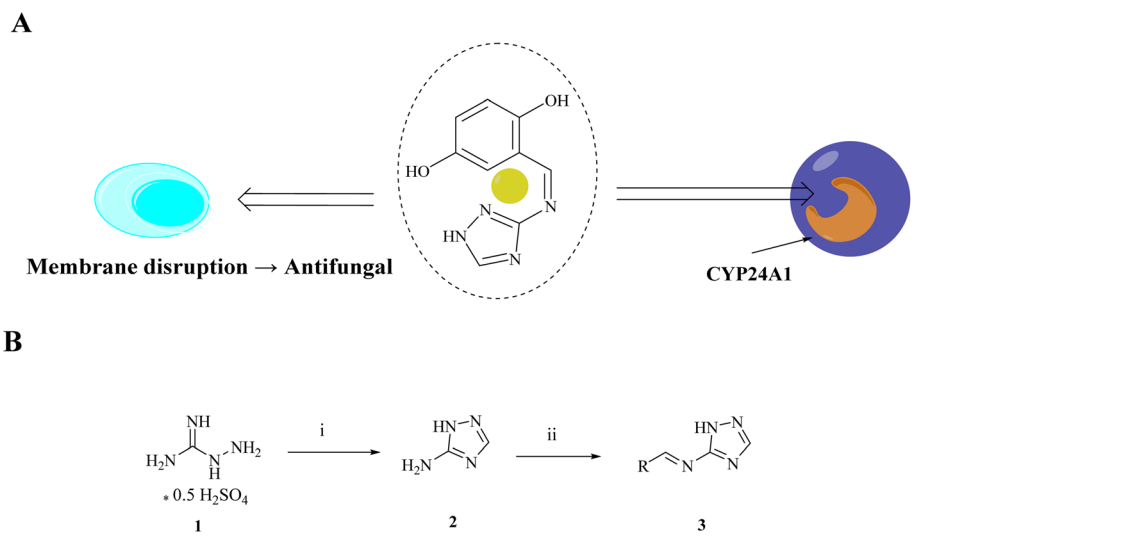

Fig. 1 Design and synthesis of triazole derivatives. (A) Design concept of triazole–Schiff base hybrid compounds. (B) Synthesis of triazole derivatives. Conditions and reagents: (i) ethanol, HCOOH, reflux, yield 82%; (ii) ethanol, different aldehyde groups, reflux, yield 73–88%.

their antibacterial efficacy was systematically evaluated using standardized minimum inhibitory concentration (MIC) assays in this study.[22] Mueller–Hinton broth was used for bacterial assays and RPMI 1640 medium for fungal assays to better reflect *in situ* bioactivity. Test strains included Gram-negative bacteria (*E. coli* ATCC 25922, *E. coli* DE17), Gram-positive bacteria (*S. aureus* ATCC 29213, MRSA2), and fungi (*C. albicans* ATCC 10231, fluconazole-resistant *C. albicans* 14053), with all procedures performed in accordance with CLSI guidelines. As summarized in Table 1, the final products **3a–3d** obtained from the reaction of 3-amino-1,2,4-triazole (**2**) with aliphatic aldehydes exhibited superior antimicrobial activity. Notably, compound **3c** demonstrated broad-spectrum antibacterial activity. In contrast, products derived from reactions of **2** with phenyl-substituted aldehydes showed weaker activity. To further verify the antifungal profile of **3c**, its activity was tested against additional fungal strains. The results, which are presented in Table 2, confirmed that compound **3c** remains active against a range of fungi, supporting its broad-spectrum antimicrobial potential.

2.3 Time–kill curve and drug-resistance studies

We further evaluated the potential clinical application value of compound **3c**. The efficacy of antifungal agents depends not

Table 1 Minimum inhibitory concentration (MIC)[a] [μg mL^{-1}] of triazole derivatives

		Negative bacteria		Positive bacteria		Fungi	
Compounds	R	*E. coli* ATCC 25922	*E. coli* DE17	*S. aureus* ATCC 29213	*S. aureus* MRSA2	*C. albicans* ATCC 10231	*C. albicans* ATCC 14053
Vancomycin[b]	—	—	—	1	2	—	—
Enrofloxacin[c]	—	0.0625	0.0625	—	—	—	—
Natamycin[d]	—	—	—	—	—	8	8
3a	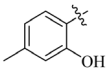	64	128	64	64	64	128
3b	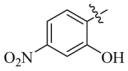	>256	>256	32	32	64	64
3c	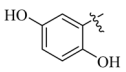	32	32	16	16	16	16
3d	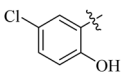	64	64	64	64	128	128
3e	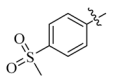	>256	>256	128	>256	128	128
3f	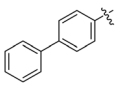	>256	>256	128	128	128	128
3g		>256	>256	256	>256	>256	>256
3h		>256	>256	256	>256	>256	>256
3i	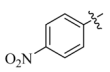	64	128	64	64	128	128
3j	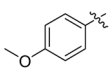	>256	>256	>256	>256	>256	>256
3k	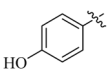	>256	>256	256	>256	>256	>256
3l	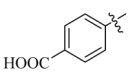	>256	>256	256	>256	>256	>256

[a] The minimum inhibitory concentration (MIC) is the lowest concentration that completely inhibits microbial growth after 16–24 hours. Experiments were repeated in triplicate. [b] Vancomycin is a clinical antibiotic for Gram-positive bacteria. [c] Enrofloxacin is a broad-spectrum quinolone antibiotic. [d] Natamycin is a natural antifungal agent produced by *Streptomyces* fermentation.

Table 2 Interaction of **3c** against varied fungal strains

Compound	*C. albicans* ATCC 90028	*C. albicans* ATCC 24433	*F. solani* 52628	*F. solani* 46492	*A. brasiliensis* TCC 16404	FO MYA 3461
Natamycin	8	8	8	8	8	8
3c	16	16	32	32	32	32

only on their initial inhibitory activity but also on their ability to delay or overcome the emergence of drug resistance, as well as to exhibit rapid and sustained fungicidal effects.[23] *Candida albicans*, as an opportunistic pathogen, possesses inherent adaptability and a rapid ability to develop resistance under drug pressure, which are key reasons for the failure of traditional single-target antifungal therapies and infection recurrence. As shown in Fig. 2A, complete inhibition of *C. albicans* ATCC 10231 growth was observed after 8 h at a concentration of 8 × MIC. Owing to the multi-target mechanism of action and membrane-disrupting properties of the Schiff base, the probability of resistance development should be low. Consistent with this, resistance studies revealed a low spontaneous mutation frequency in *C. albicans* ATCC 10231 against **3c**. As illustrated in Fig. 2B, after 28 serial passages, the MIC value increased by no more than 8-fold. These results demonstrate that compound **3c** not only effectively kills fungi but also minimizes the risk of resistance development.

2.4 Cytotoxicity against mammalian cells

To determine whether the broad-spectrum antifungal effects of compound **3c** stem from general cytotoxicity or fungus-specific toxicity, its cytotoxicity was evaluated using human umbilical vein endothelial cells (HUVECs) and Caco-2 intestinal epithelial cells *via* the CCK-8 assay.[22] As shown in Fig. 3, treatment with compound **3c** resulted in cell viability above 80% at 128 μg mL^{-1} and above 95% at 64 μg mL^{-1} for both HUVECs and Caco-2 cells, indicating low cytotoxicity and a favorable safety profile.

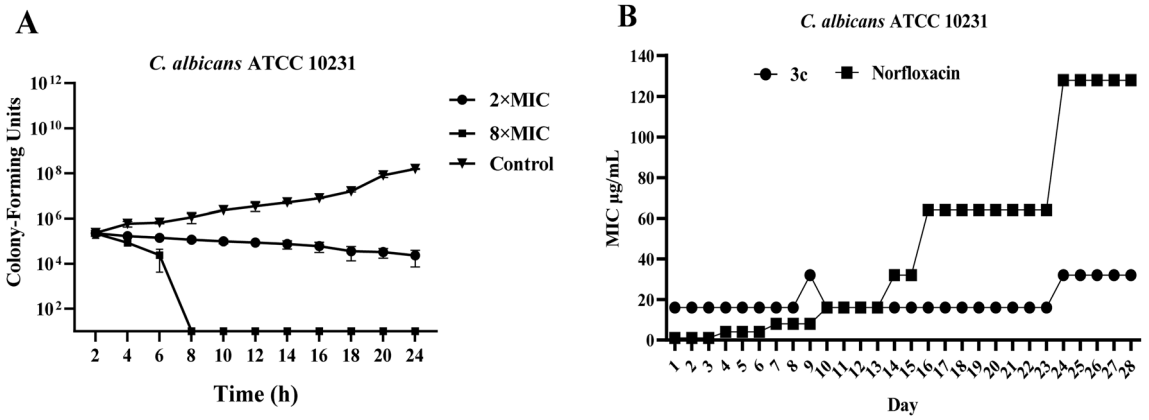

Fig. 2 (A) Time–kill kinetics of **3c** against *C. albicans* ATCC 10231. (B) Resistance development of **3c**. Data are presented as means ± SEM (standard error of mean) from three independent experiments. Norfloxacin was used as a reference drug.

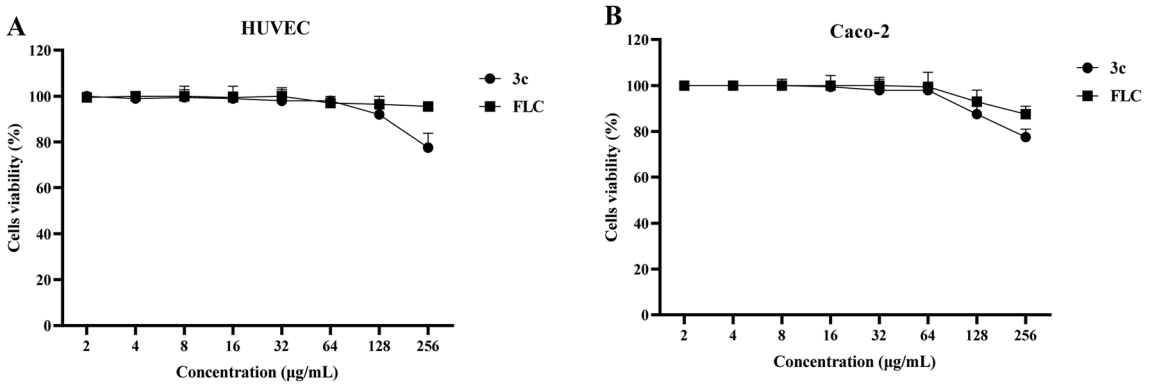

Fig. 3 *In vitro* cytotoxicity evaluation of **3c** in HUVEC (A) and Caco-2 (B) cells was assessed using the CCK-8 assay. Results represent the means ± standard deviations from three experiments. FLC – fluconazole.

2.5 Hemolysis assay

A hemolysis assay was subsequently performed for compound **3c**. Rigorous evaluation of the hemolytic potential of candidate compounds is not only a reflection of scientific rigor in drug development but also a critical step for early assessment of clinical translation prospects and potential risks.[24] Using 1% Triton X-100 solution as the positive control and sterile PBS as the negative control, no significant hemolysis was observed for compound **3c** within the concentration range of 16–128 μg mL^{-1}, as shown in Fig. 4. The half hemolytic concentration (HC_{50}) was not reached even at 256 μg mL^{-1}. These results indicate that **3c** exhibits no hemolytic activity against rabbit red blood cells at concentrations effective for its antimicrobial action.

2.6 Antifungal mechanism

Schiff base compounds can disrupt the integrity of the fungal plasma membrane through electrostatic interactions. To determine the mode of antifungal action of these compounds, their effect on membrane integrity in live fungal cells was assessed using SYTOX Green nucleic acid staining.[25] SYTOX Green is a DNA-binding dye that readily penetrates the damaged membranes of dead cells but cannot cross the intact membranes of viable cells. After treating a *C. albicans* ATCC 10231 cell suspension with compound **3c** at 4 × MIC, the fluorescence intensity was monitored. As shown in Fig. 5A, a gradual increase in fluorescence was observed over 20 min, indicating that **3c** directly compromises fungal membrane integrity. To further confirm that the mode of action of **3c** is membrane-targeted, the leakage of calcein from large unilamellar vesicles (LUVs) was measured (Fig. 5B). Calcein-loaded liposomes composed of DOPC/DOPE/PI (2 : 1 : 1) with 15 wt% ergosterol were used to mimic negatively charged fungal membranes. Compound **3c** induced leakage of the contents in a dose-dependent manner, confirming our hypothesis.

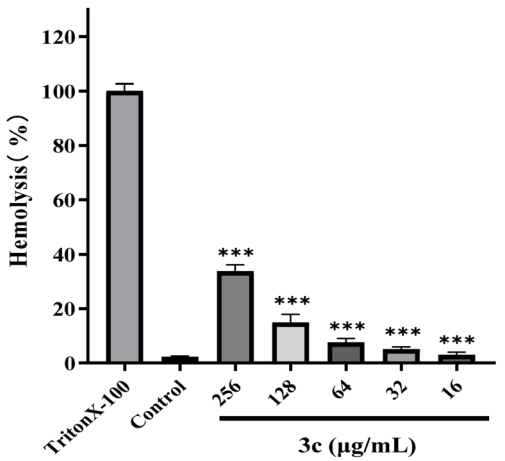

Fig. 4 Percentage hemolysis of rabbit blood cells at various **3c** concentrations. Asterisks indicate differences considered to be significant at the *$p < 0.05$, **$p < 0.01$, and ***$p < 0.001$ levels.

2.7 Inhibitory effects towards *C. albicans* biofilm formation

To address the core clinical challenge of stubborn biofilms formed by *Candida albicans* and other pathogens in mixed female reproductive tract infections, we evaluated the ability of compound **3c** to inhibit and eradicate these structures. This study aims to overcome the limitations of current therapies that target only planktonic pathogens but fail to eliminate biofilms by directly investigating whether **3c** can disrupt the symbiotic network among pathogens. Our work provides critical experimental evidence for the development of novel multi-target therapeutic strategies capable of penetrating biofilm barriers. As shown in Fig. 6, compound **3c** exhibited strong antifungal biofilm activity *in vitro*. It not only effectively inhibited the formation of *C. albicans* biofilms but also significantly disrupted pre-formed mature biofilms. This dual efficacy suggests that **3c** has the potential to directly overcome the physical and drug-resistance barriers constructed by biofilm consortia in mixed infections. Its unique mechanism lays a solid foundation for developing novel treatments against recurrent VVC/BV co-

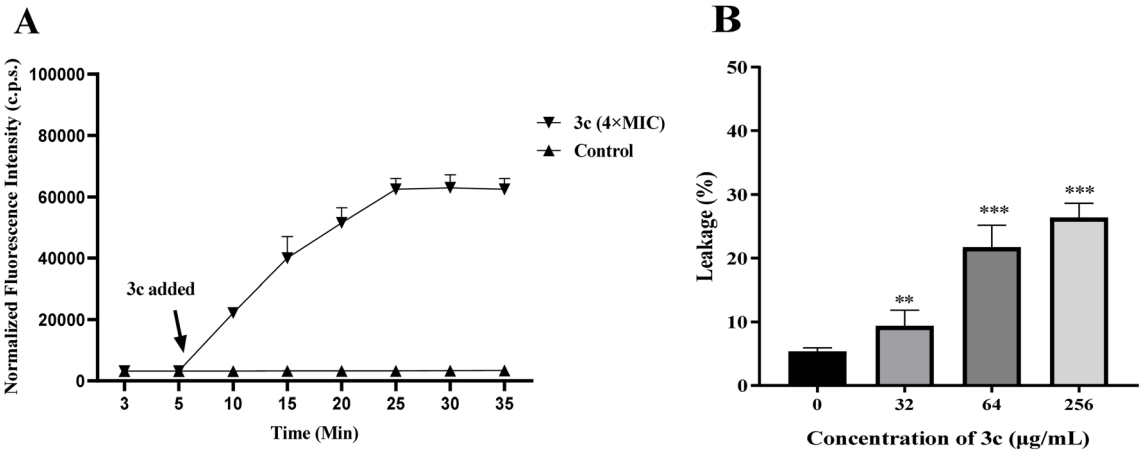

Fig. 5 (A) Membrane-permeabilizing properties of compound **3c** at 4 × MIC against *C. albicans* ATCC 10231. (B) Percentage calcein leakage from calcein-loaded LUVs induced by compound **3c**. The investigated liposome with the composition DOPC/DOPE/PI = 2 : 1 : 1 containing 15% ergosterol was used to mimic fungal membranes.

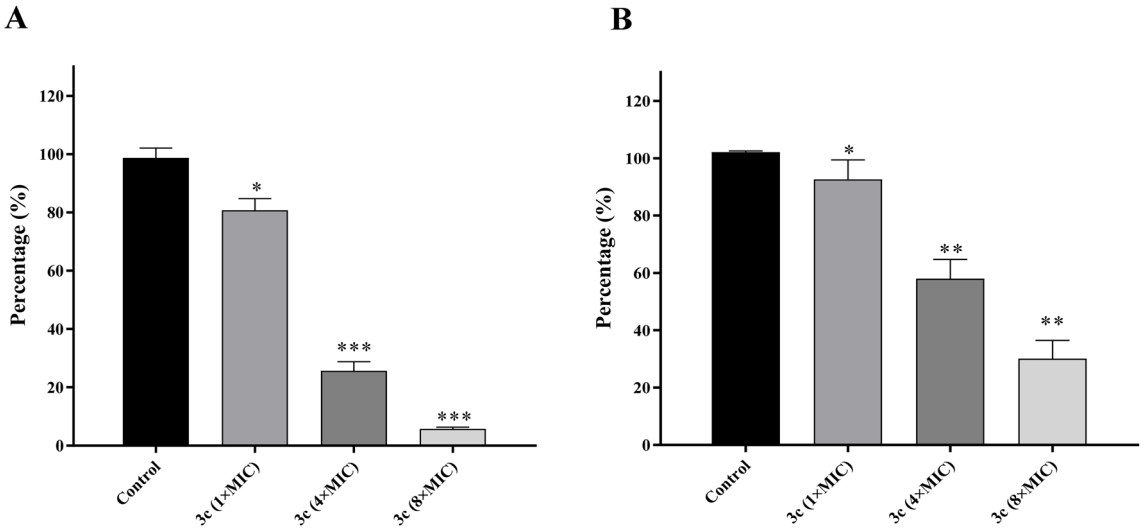

Fig. 6 (A) Inhibition rate of **3c** on *C. albicans* ATCC 10231 biofilm formation. (B) Biofilm dispersion of **3c** on *C. albicans* ATCC 10231 biofilm. Asterisks indicate differences considered to be significant at the $*p < 0.05$, $**p < 0.01$, and $***p < 0.001$ levels.

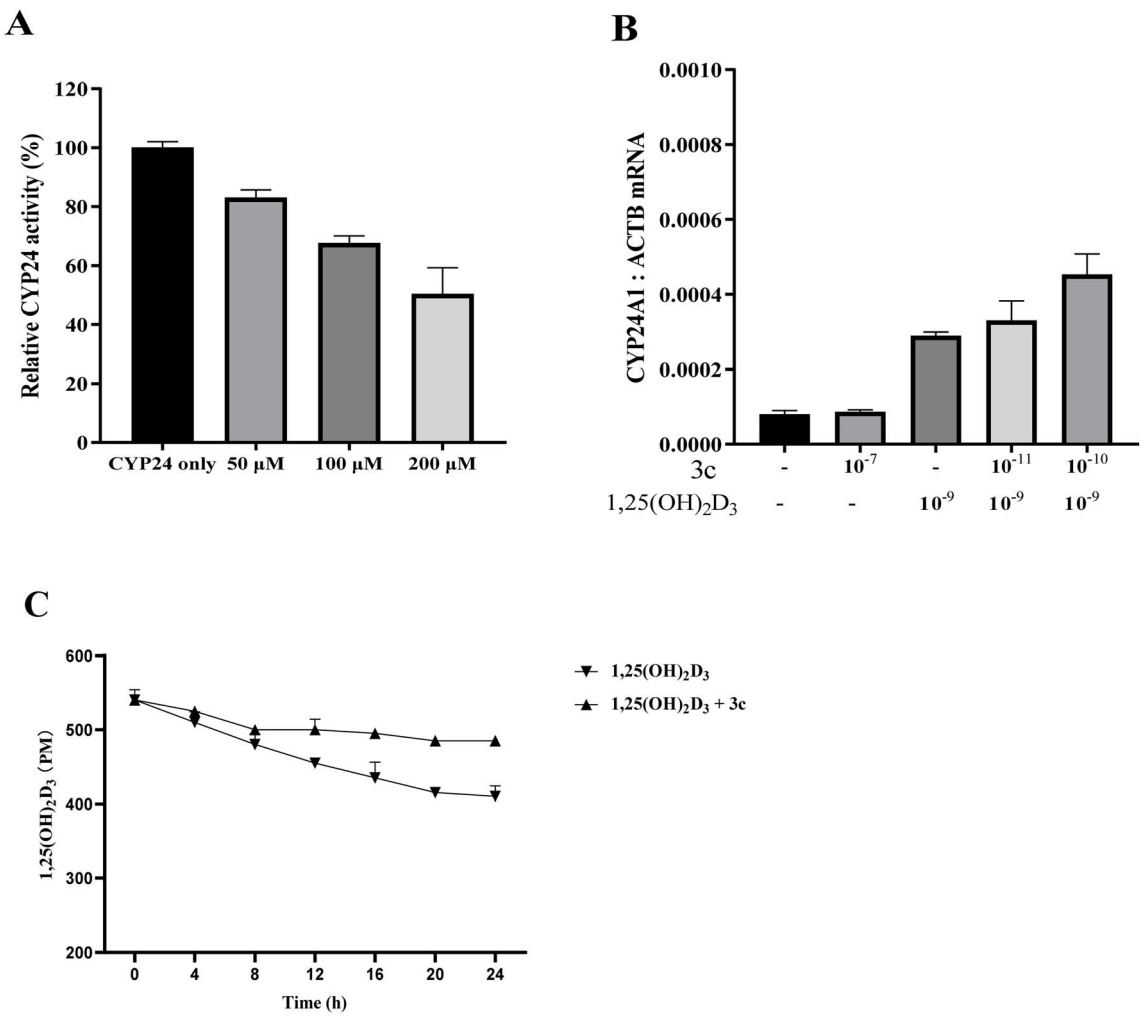

Fig. 7 (A) *In vitro* CYP24-inhibition efficacy of aptamers. (B) Effect of the combination of **3c** and $1,25(OH)_2D_3$ on the mRNA levels of CYP24A1 in HEK293T cell culture at 24 h. (C) Levels of $1,25(OH)_2D_3$ in HEK293T cell culture in the absence and presence of **3c**. Data are presented as means ± SD from three independent experiments.

infections that combine both biofilm-disrupting and antimicrobial functions into a single agent.

2.8 Evaluation of CYP24A1 inhibition

The biological activity of vitamin D_3 in humans is primarily regulated by the enzymatic activity of cytochrome P450 24-hydroxylase (CYP24A1). This enzyme catalyzes the hydroxylation of both 25-hydroxyvitamin D_3 ($25(OH)D_3$) and 1,25-dihydroxyvitamin D_3 ($1,25(OH)_2D_3$), which represents the initial step in vitamin D catabolism.[26] The pathological upregulation of CYP24A1 has been observed in various diseases. Specifically, within the vaginal infection microenvironment, aberrant overexpression of CYP24A1 leads to rapid degradation of active vitamin D into the functionally inert $24,25\text{-}(OH)_2D_3$, highlighting the importance of developing CYP24A1 inhibitors.[27]

As shown in Fig. 7A, *in vitro* evaluation revealed that target compound **3c** inhibits CYP24A1 by 32% at 100 μM, with an IC_{50} of 202 μM. Despite its lower potency compared to azole inhibitors like VID400, compound **3c** offers a favorable profile of lower toxicity and superior antifungal activity. Fig. 7B and S1 present the comparative effects of compound **3c**, both alone and in combination with $1,25(OH)_2D_3$, on CYP24A1 mRNA levels in HEK293T cells. The results demonstrate that, at a concentration of 10^{-7} M, compound **3c** did not alter CYP24A1 mRNA expression compared to the solvent control. In contrast, treatment with 10^{-9} M $1,25(OH)_2D_3$ for 24 h significantly increased CYP24A1 mRNA levels. Furthermore, when cells were co-treated with compound **3c** (10^{-10} M) and $1,25(OH)_2D_3$ (10^{-9} M) for 24 h, CYP24A1 mRNA expression was markedly enhanced relative to treatment with $1,25(OH)_2D_3$ alone. Finally, LC-MS/MS analysis was performed to quantify changes in the concentration of $1,25(OH)_2D_3$ in HEK293T cell cultures in the presence or absence of 10^{-7} M compound **3c** (Fig. 7C). In the absence of compound **3c**, the concentration of $1,25(OH)_2D_3$ decreased rapidly within 8 h. In contrast, the degradation rate was significantly slowed in the presence of compound **3c**, with the average concentration of $1,25(OH)_2D_3$ remaining at 495 pM after 24 h. Our results demonstrate that compound **3c** is a potent CYP24A1 inhibitor with strong enzyme-suppressing characteristics, providing an important experimental basis for the further development of drugs targeting the CYP24A1 inhibition mechanism.

3. Conclusion

In this study, a series of "triazole–Schiff base" hybrid compounds were synthesized with the aim of comprehensively addressing the dual challenges of biofilm-associated drug resistance and dysregulated local immune microenvironment in mixed female reproductive tract infections *via* a multi-mechanism synergistic strategy. Among them, the lead compound **3c** demonstrated outstanding performance. It not only exhibited broad-spectrum antimicrobial activity against various bacteria and fungi (with a minimum inhibitory concentration, MIC, of 16 μg mL^{-1}) but also showed low mammalian cell cytotoxicity. Moreover, it significantly inhibited the formation of *C. albicans* biofilms and effectively eradicated established mature biofilms, demonstrating potential against stubborn biofilm-associated infections. At the mechanistic level, studies revealed that compound **3c** possesses dual pharmacological effects: it both directly disrupts microbial cell structures through membrane-targeting action, rapidly killing pathogens, and effectively inhibits CYP24A1 enzyme activity, achieving a 32% inhibition rate at a concentration of 100 μM. More importantly, in cellular models, a low concentration (10^{-7} M) of this compound significantly delayed the metabolic clearance of active vitamin D ($1,25(OH)_2D_3$), prolonging its half-life. After 24 h, the concentration of $1,25(OH)_2D_3$ in the culture medium remained at an effective level of 495 pM, thereby enhancing the function of the vitamin D–VDR signaling pathway, upregulating antimicrobial peptide expression, and improving the local immune microenvironment at the infection site.

While this study confirms the multi-target anti-infective potential of compound **3c** at the cellular and enzymatic levels, its clinical translation will require further validation through *in vivo* studies and more complex infection models. We also acknowledge that the lack of synergy testing between compound **3c** and existing standard therapies is an important limitation of this work. Future research will prioritize establishing polymicrobial biofilm models and animal infection models to comprehensively evaluate the efficacy of compound **3c** under conditions that better reflect the clinical reality. Additionally, assessing its synergistic effects with commonly used clinical anti-infective agents to explore potential combination therapies will be a key focus of future investigations. Furthermore, to advance compound **3c** toward clinical application, several formulation challenges must be addressed: its poor aqueous solubility may limit bioavailability in local vaginal formulations such as gels or suppositories. Subsequent studies should include systematic pre-formulation work, including evaluation of its chemical stability across physiologically relevant pH values (4.0–7.4) and at various storage temperatures, as well as the development of suitable delivery systems (*e.g.*, nanocrystals, liposomes, or polymeric microparticles) to improve its solubility, stability, and tissue penetration. Overcoming these formulation hurdles will be essential for accelerating the translational development of compound **3c**. In summary, compound **3c** innovatively integrates the synergistic mechanisms of "direct antimicrobial action, biofilm penetration, and immunomodulation." It not only effectively overcomes the limitations of traditional antimicrobial agents—such as ineffectiveness against biofilms and propensity toward the development of resistance—but also enhances overall anti-infective efficacy by modulating host immune responses. This provides a promising drug candidate with broad translational potential for the clinical treatment of mixed infections.

4. Experimental section

4.1 Chemical synthesis

All chemicals were of reagent grade or higher, and were obtained from Adamas and used without further purification.

Solvents were used as supplied or dried over molecular sieves when required. Column chromatography utilized silica gel (100–200 mesh, Qingdao Ocean Chemical). Reactions were monitored by TLC on silica gel GF254 plates (Yantai Jiangyou). ^{1}H NMR (400 MHz) and ^{13}C NMR (100 MHz) spectra were recorded on a Bruker Avance 400 spectrometer; chemical shifts are referenced to residual solvent peaks (DMSO: δ_H 2.50, δ_C 39.52). High-resolution mass spectra (HRMS) were obtained using an AB Sciex TripleTOF 5600+ instrument with ESI ionization.

4.1.1 1*H*-1,2,4-Triazol-3-amine (2). To a solution of aminoguanidine **1** (7.5 mmol) in water (5 mL), sodium hydroxide (7.5 mmol) was added, and the mixture was stirred for 10 min. Subsequently, formic acid (7.40 mmol) was introduced, and the reaction mixture was heated at 80 °C until complete dissolution was achieved, followed by further reaction at 120 °C for 6 h. The reaction was quenched by the addition of ice water. The resulting mixture was then subjected to recrystallization from ethanol to afford **2**. 68.9 mg, yield, 82%. White solid powder. M.P. 150.5–153.2 °C. ^{1}H NMR (400 MHz, DMSO-d_6) δ 7.46 (s, 1H), 5.77 (s, 2H).

4.1.2 2-{[(1*H*-1,2,4-Triazol-3-yl)imino]methyl}-5-methylphenol (3a). Product **2** (1 mmol) was dissolved in anhydrous ethanol and treated with aldehyde derivatives bearing various substituents; the mixture was then refluxed for 8 h. After completion of the reaction, the solution was concentrated under reduced pressure. The final product **3** was obtained by recrystallization from ethanol.

161.6 mg, yield, 80%. White solid powder. M.P. 147.5–149.5 °C. ^{1}H NMR (400 MHz, DMSO-d_6) δ 12.50 (s, 1H), 9.62 (s, 1H), 8.81 (s, 1H), 7.80 (s, 1H), 7.49 (d, J = 8.0 Hz, 1H), 7.12 (d, J = 8.4 Hz, 1H), 2.73 (s, 2H). ^{13}C NMR (101 MHz, DMSO-d_6) δ 191.75, 164.66, 144.28, 137.23, 134.79, 132.12, 128.86, 128.08, 118.80, 116.57, 56.03, 19.91. TOF-MS, m/z: [M + H]$^+$, calcd for $C_{10}H_{11}N_4O^+$, 203.0933, found: 203.0937.

4.1.3 2-{[(1*H*-1,2,4-Triazol-3-yl)imino]methyl}-5-nitrophenol (3b). 180.6 mg, yield, 81%. White solid powder. M.P. 202.5–204.5 °C. ^{1}H NMR (400 MHz, DMSO-d_6) δ 9.51 (s, 1H), 8.78 (s, 1H), 8.25 (d, J = 12.0 Hz, 1H), 7.14 (d, J = 9.1 Hz, 1H). ^{13}C NMR (101 MHz, DMSO-d_6) δ 165.69, 162.04, 140.28, 131.06, 129.22, 126.92, 124.85, 120.24, 118.22. TOF-MS, m/z: [M + H]$^+$, calcd for $C_9H_8N_5O_3^+$, 224.0627, found: 224.0629.

4.1.4 2-{[(1*H*-1,2,4-Triazol-5-yl)imino]methyl}benzene-1,4-diol (3c). 169.3 mg, yield, 83%. White solid powder. M.P. 151.5–153.5 °C. ^{1}H NMR (400 MHz, DMSO-d_6) δ 11.66 (s, 1H), 9.32 (s, 1H), 9.11 (s, 1H), 8.56 (s, 1H), 7.15 (s, 1H), 6.96–6.79 (m, 2H), 3.36 (s, 1H). ^{13}C NMR (101 MHz, DMSO-d_6) δ 164.43, 153.43, 150.06, 144.42, 124.74, 122.11, 119.50, 117.58, 116.51. TOF-MS, m/z: [M + H]$^+$, calcd for $C_9H_9N_4O_2^+$, 205.0725, found: 205.0727.

4.1.5 2-{[(1*H*-1,2,4-Triazol-5-yl)imino]methyl}-4-chlorophenol (3d). 162.1 mg, yield, 73%. White solid powder. M.P. 152.5–154.5 °C. ^{1}H NMR (400 MHz, DMSO-d_6) δ 9.42 (s, 1H), 7.89 (d, J = 2.7 Hz, 1H), 7.46 (dd, J = 8.8, 2.6 Hz, 1H), 7.02 (d, J = 8.8 Hz, 1H). ^{13}C NMR (101 MHz, DMSO-d_6) δ 190.13, 163.24, 159.92, 159.27, 136.14, 127.78, 123.89, 119.94, 119.15. TOF-MS, m/z: [M + H]$^+$, calcd for $C_9H_8ClN_4O^+$, 223.0386, found: 223.0388.

4.1.6 1-[4-(Methylsulfonyl)phenyl]-*N*-(1*H*-1,2,4-triazol-5-yl) methanimine (3e). 220.1 mg, yield, 88%. White solid powder. M.P. 181.5–183.5 °C. ^{1}H NMR (400 MHz, DMSO-d_6) δ 9.33 (s, 1H), 8.26 (d, J = 8.1 Hz, 2H), 8.15 (s, 1H), 8.08 (d, J = 8.1 Hz, 2H), 7.65 (s, 1H), 3.29 (s, 3H). ^{13}C NMR (101 MHz, DMSO-d_6) δ 193.05, 192.85, 145.52, 139.50, 130.42, 129.94, 127.95, 127.74, 43.51. TOF-MS, m/z: [M + H]$^+$, calcd for $C_{10}H_{11}N_4O_2S^+$, 251.0602, found: 251.0605.

4.1.7 1-[(1,1′-Biphenyl)-4-yl]-*N*-(1*H*-1,2,4-triazol-5-yl) methanimine (3f). 210.8 mg, yield, 85%. White solid powder. M.P. 177.5–179.5 °C. ^{1}H NMR (400 MHz, DMSO-d_6) δ 9.28 (d, J = 7.6 Hz, 1H), 8.55 (s, 1H), 8.10 (t, J = 8.3 Hz, 2H), 7.86 (t, J = 9.9 Hz, 2H), 7.77 (d, J = 7.5 Hz, 2H), 7.51 (t, J = 7.5 Hz, 2H), 7.43 (d, J = 6.9 Hz, 1H). ^{13}C NMR (101 MHz, DMSO-d_6) δ 166.42, 165.27, 162.91, 151.23, 144.15, 143.70, 139.38, 134.79, 130.37, 129.86, 129.29, 128.38, 127.49, 127.09. TOF-MS, m/z: [M + H]$^+$, calcd for $C_{15}H_{13}N_4^+$, 249.1140, found: 249.1143.

4.1.8 1-(4-Chlorophenyl)-*N*-(1*H*-1,2,4-triazol-5-yl) methanimine (3g). 154.8 mg, yield, 80%. White solid powder. M.P. 135.5–137.5 °C. ^{1}H NMR (400 MHz, DMSO-d_6) δ 9.23 (s, 1H), 8.03 (d, J = 7.9 Hz, 2H), 7.61 (d, J = 7.2 Hz, 2H). ^{13}C NMR (101 MHz, DMSO-d_6) δ 160.79, 158.81, 149.50, 136.33, 133.62, 130.33, 128.69, 124.25. TOF-MS, m/z: [M + H]$^+$, calcd for $C_9H_8ClN_4^+$, 207.0617, found: 207.0619.

4.1.9 1-(Pyridin-4-yl)-*N*-(1*H*-1,2,4-triazol-5-yl)methanimine (3h). 141.8 mg, yield, 82%. White solid powder. M.P. 137.5–139.5 °C. ^{1}H NMR (400 MHz, DMSO-d_6) δ 9.26 (s, 1H), 8.91–8.86 (m, 1H), 8.78 (d, J = 5.3 Hz, 2H), 7.91 (s, 2H), 7.85–7.78 (m, 1H). ^{13}C NMR (101 MHz, DMSO-d_6) δ 160.63, 158.52, 149.60, 146.22, 144.60, 124.48, 114.95. TOF-MS, m/z: [M + H]$^+$, calcd for $C_8H_8N_5^+$, 174.0779, found: 174.0783.

4.1.10 1-(4-Nitrophenyl)-*N*-(1*H*-1,2,4-triazol-5-yl) methanimine (3i). 173.6 mg, yield, 80%. White solid powder. M.P. 157.5–159.5 °C. ^{1}H NMR (400 MHz, DMSO-d_6) δ 9.36 (s, 1H), 8.36 (d, J = 8.6 Hz, 2H), 8.27 (d, J = 8.6 Hz, 2H). ^{13}C NMR (101 MHz, DMSO-d_6) δ 161.97, 159.70, 151.35, 149.77, 141.33, 128.96, 124.51. TOF-MS, m/z: [M + H]$^+$, calcd for $C_9H_8N_5O_2^+$, 218.0678, found: 218.0679.

4.1.11 1-(4-Methoxyphenyl)-*N*-(1*H*-1,2,4-triazol-5-yl) methanimine (3j). 171.7 mg, yield, 85%. White solid powder. M.P. 124.5–126.5 °C. ^{1}H NMR (400 MHz, DMSO-d_6) δ 9.14 (s, 1H), 7.95 (d, J = 7.4 Hz, 2H), 7.07 (d, J = 7.9 Hz, 2H), 3.83 (s, 3H). ^{13}C NMR (101 MHz, DMSO-d_6) δ 163.82, 162.06, 150.49, 143.29, 131.40, 130.48, 129.25, 114.09, 55.26. TOF-MS, m/z: [M + H]$^+$, calcd for $C_{10}H_{11}N_4O^+$, 203.0933, found: 203.0937.

4.1.12 4-{[(1*H*-1,2,4-Triazol-5-yl)imino]methyl}phenol (3k). 161.7 mg, yield, 86%. White solid powder. M.P. 134.5–136.5 °C. ^{1}H NMR (400 MHz, DMSO-d_6) δ 9.08 (s, 1H), 7.85 (d, J = 8.4 Hz, 2H), 6.91 (d, J = 8.3 Hz, 2H). ^{13}C NMR (101 MHz, DMSO-d_6) δ 163.75, 161.84, 137.74, 135.56, 132.53, 129.12, 116.28. TOF-MS, m/z: [M + H]$^+$, calcd for $C_9H_9N_4O^+$, 189.0776, found: 189.0779.

4.1.13 4-{[(1*H*-1,2,4-Triazol-5-yl)imino]methyl}benzoic acid (3l). 187.9 mg, yield, 87%. White solid powder. M.P. 206.5–208.5 °C. ^{1}H NMR (400 MHz, DMSO-d_6) δ 9.29 (s, 1H), 8.10 (q, J = 8.2 Hz, 4H). ^{13}C NMR (101 MHz, DMSO-d_6) δ 170.51, 160.49,

158.70, 149.37, 141.76, 130.11, 127.53, 124.48. TOF-MS, *m*/*z*: $[M + H]^+$, calcd for $C_{10}H_9N_4O_2^+$, 217.0725, found: 217.0733.

4.2 Determination of minimum inhibitory concentration

4.2.1 Fungi. The *in vitro* antifungal activity of the target compounds was tested using the broth microdilution method recommended by CLSI (M27-A3). Fungi in the exponential growth phase were collected in 1.5 mL centrifuge tubes and washed three times with 1 mL of phosphate-buffered saline (PBS). A fungal suspension with a concentration of 1×10^3 CFU mL^{-1} was then prepared using RPMI 1640 medium. The test compounds and FLC were added to a 96-well plate, with each concentration tested in triplicate wells, followed by serial twofold dilutions. The optical density (OD_{600}) at 600 nm was measured using a microplate reader to calculate the MIC values of the test compounds.[22]

4.2.2 Bacteria. All compounds were dissolved in dimethyl sulfoxide (DMSO; final DMSO concentration less than 0.5%) and sterile double-distilled water and then diluted with Mueller–Hinton broth (MHB). The stock solutions of each compound were serially diluted twofold to obtain concentration ranges from 1 to 256 μg mL^{-1}. All bacterial cell suspensions were adjusted in MHB to achieve a starting inoculum of 1×10^6 cells per mL. A total volume of 100 μL of the bacterial suspension was then added to each well. After incubation at 37 °C, the optical density at 600 nm (OD_{600}) was measured using a BioTek microplate reader. The MIC was defined as the lowest concentration of the antibiotic/compound that completely inhibited microbial growth.[28]

4.3 Time–killing kinetics

The time–kill assay was performed as described previously. Fungal cells in the exponential growth phase were collected and diluted with RPMI 1640 medium to a concentration of 1.5×10^6 cells per mL. The cell suspension was aliquoted into Eppendorf tubes, with 5 mL per tube, followed by the addition of the drug. The tubes were then incubated with shaking at 200 rpm at 30 °C. From each tube, 100 μL of the fungal cell culture medium was aspirated and transferred to a 96-well microtiter plate. After incubation at 37 °C, the optical density at 600 nm (OD_{600}) of each well was measured to calculate the concentration of fungal cells.[22]

4.4 Drug-resistance study

The drug-resistance study of compound **3c** was conducted according to a previously reported experimental protocol. The initial minimum inhibitory concentration (MIC) of **3c** against *C. albicans* was determined using the method described above, and the assay was repeated continuously for 28 days.[29]

4.5 Cytotoxicity assay

The cytotoxic effects of the compounds on the viability of human umbilical vein endothelial cells (HUVECs) and Caco-2 intestinal epithelial cells were evaluated using the Cell Counting Kit-8 (CCK-8) assay, as previously described. Briefly, HUVECs or Caco-2 cells (1×10^4 cells per well) were seeded into 96-well microtiter plates and cultured in DMEM medium (HyClone) supplemented with 10% FBS (HyClone) for 3 h to allow adhesion. After removing the supernatant, fresh DMEM medium containing different concentrations of the compounds (4–256 μg mL^{-1}) was added, followed by incubation at 37 °C for 24 h. Then, CCK-8 solution (10 μL per well) was added, and the cells were incubated for another 2 h at 37 °C. The absorbance at 450 nm was measured using an ELISA microplate reader. Cells incubated in DMEM containing only DMSO (<1% of the total assay volume) served as the 100% viability control.[22]

4.6 Hemolysis assay

The hemolysis assay was performed as described previously. Rabbit erythrocytes (4% v/v suspension in PBS) were mixed with equal volumes (100 μL each) of C5 in PBS, resulting in final C5 concentrations of 2–256 μg mL^{-1}. Controls included 1% Triton X-100 (positive control) and PBS (negative control). After incubation at 37 °C for 1 h, the samples were centrifuged (1000*g*, 5 min). The absorbance of the supernatant was then measured at 490 nm. Hemolysis (%) was calculated using the formula: Hemolysis (%) = [(sample − PBS)/(Triton − PBS)] × 100. All experiments were performed in triplicate.[22]

4.7 Assessment of biofilm formation and inhibitory activity

Fungal cells in the exponential growth phase were collected and diluted with RPMI 1640 medium to a concentration of 1×10^6 CFU mL^{-1}. The fungal suspension was then added to a 96-well plate. The plate was incubated at 37 °C for 1.5 h to promote biofilm adhesion. After incubation, the supernatant was aspirated, and the adhered biofilms were gently washed twice with PBS to remove non-adherent cells. Fresh RPMI 1640 medium containing different concentrations of the test compounds was subsequently added to the wells, and the plate was further incubated in the dark at 37 °C for 24 h. The adherent cells were then stained at 37 °C for 3 h. Finally, the optical density (OD) of the stained fungal cells in the 96-well plate was measured using a microplate reader to calculate the inhibition rate of the test compounds on fungal biofilm formation.

For the biofilm eradication assay, standard *Candida* strains (*e.g.*, *Candida albicans* ATCC 10231) were first cultured overnight in liquid medium, and the bacterial suspension was adjusted to 1×10^6 to 1×10^7 CFU mL^{-1} using a spectrophotometer. Then, 100 μL of the fungal suspension was added to each well of a 96-well flat-bottom cell culture plate and incubated statically at 37 °C for 24 h to form mature biofilms. After discarding the supernatant, the biofilms were gently rinsed twice with PBS to remove non-adherent planktonic cells. Fresh medium (100 μL) containing different concentrations of the test compounds was added to the experimental wells, with positive control wells receiving standard drugs such as amphotericin B and negative control wells containing only the medium. The plate was further incubated at 37 °C for 24 h for eradication treatment. After treatment, the drug solution was discarded, and the biofilms were rinsed again with PBS. Then, a 0.1% crystal violet solution was added to each well for staining. After

15 min of incubation, excess dye was removed by washing. Subsequently, 95% ethanol was added to dissolve the crystal violet bound to the biofilms. The optical density at 590 nm (OD_{590}) was measured using a microplate reader. The biofilm eradication rate was calculated by comparing the OD values of the experimental groups with those of the negative control group (representing the maximum biofilm biomass) using the formula: Eradication rate (%) = [1 − (OD_experimental/OD_negative control)] × 100%.[30]

4.8 SYTOX Green assay

The SYTOX Green assay was used to measure changes in the membrane integrity of *Candida albicans* after treatment with the compounds. The assay was performed as previously described with some modifications. Briefly, an overnight culture of *C. albicans* was washed three times with PBS buffer and resuspended in PBS to an OD_{600} of 0.2. The yeast suspension was incubated with 0.3 μM SYTOX Green dye in the dark, followed by the addition of the compounds. After the fluorescence signal of the SYTOX Green-treated suspension reached a stable plateau, xanthone compounds dissolved in PBS/DMF (final DMF concentration = 0.5%) were added. The increase in fluorescence was continuously monitored for 1–2 hours using a PTI spectrofluorometer (excitation wavelength: 504 nm; emission wavelength: 523 nm).[25]

4.9 Calcein leakage assay

Liposomes composed of DOPC/DOPE/PI (2 : 1 : 1) containing 15 wt% ergosterol were used to mimic fungal membranes. Large unilamellar vesicles (LUVs) were prepared using the membrane hydration method, as previously described. Briefly, lipids were dissolved in chloroform/methanol and lyophilized overnight. The dried lipid film was then hydrated with a dye solution (80 mM calcein, 50 mM HEPES, 100 mM NaCl, and 0.3 mM EDTA, pH 7.4) and vortexed. The lipid mixture was subjected to 10 freeze–thaw cycles and extruded 10 times through a polycarbonate filter (100 nm pore size) to produce uniform calcein-loaded LUVs with an average diameter of approximately 100 nm. Untrapped calcein was removed by gel filtration on a Sephadex G-50 column using HEPES buffer as the eluent. The concentration of calcein-loaded LUVs was determined using a total phosphorus assay. Compound **3c** dissolved in HEPES buffer containing 5% (v/v) DMF/HEPES buffer at the desired concentration was added to the calcein-loaded LUV solution. Leakage of calcein from the LUVs was monitored by measuring the fluorescence emission intensity at 520 nm with excitation at 490 nm using a TECAN Infinite M200 Pro-microplate reader. The percentage calcein leakage was calculated according to the following equation: % calcein leakage = $[(F_t - F_{min})/(F_{max} - F_{min})] \times 100$, where F_t represents the fluorescence intensity after addition of the test compound, F_{min} is the fluorescence intensity of untreated LUVs, and F_{max} is the fluorescence intensity after treatment with 1% Triton X-100.[25]

4.10 Assessment of relevant genetic response to 3c

After the HEK293T cells reached adherence, experimental replicates were set up as follows: control group (0.2% v/v ethanol), compound **3c** (10^{-7} M) only treatment group, $1,25(OH)_2D_3$ (10^{-9} M) only treatment group, and treatment groups using a combination of compound **3c** (10^{-11} M or 10^{-10} M) with $1,25(OH)_2D_3$ (10^{-9} M). All treatments were administered for 24 hours. Replicates for each group were designated for RNA extraction, which was performed using TRIzol® reagent (Thermo Fisher Scientific) according to the manufacturer's instructions. The brief procedure is as follows: after removing the culture medium, 200 μL of TRIzol® was added directly to each well to lyse the cells. The lysate was transferred to a 1.5 mL centrifuge tube, mixed with 40 μL of chloroform, vigorously shaken, and then centrifuged at 4 °C and 12 000*g* for 15 min. The aqueous phase was transferred to a new tube, mixed with 100 μL of isopropanol to precipitate the RNA, allowed to stand for 10 min, and then centrifuged at 4 °C and 12 000*g* for 10 min. The supernatant was discarded, and the RNA pellet was washed with 200 μL of 70% ethanol, vortexed for 5 s, and centrifuged at 4 °C and 7500*g* for 5 min. After discarding the ethanol, the pellet was air-dried for 10 min. Finally, the RNA was resuspended in 25 μL of RNase-free water, incubated in a 60 °C water bath for 10 min, and stored at −80 °C for future use.

The extracted total RNA samples were used to quantify the expression of CYP24A1 mRNA and the housekeeping gene ACTB *via* quantitative PCR. For reverse transcription, 2 μg of total RNA was used with the iScript™ cDNA Synthesis Kit (Bio-Rad). Then, 12.5 ng of cDNA was subjected to real-time quantitative PCR using Forget-Me-Not™ EvaGreen® qPCR Mastermix (Biotium) to analyze the mRNA expression levels of the target genes.[27]

4.11 CYP24-inhibition assay

The aptamer-mediated CYP24 inhibition assay was performed using a previously reported membrane-reconstituted system. The reaction mixture contained 0.5 μM adrenodoxin (ADX), 0.05 μM adrenodoxin reductase (ADR), and 5 nM CYP24 in a buffer consisting of 100 mM Tris–HCl (pH 7.4) and 1 mM EDTA. Compound **3c** was added at concentrations ranging from 50 to 200 μM, and the mixture was reacted at room temperature (RT) for 15 min to assess the concentration-dependent CYP24 inhibitory activity. After the addition of compound **3c**, the reaction mixture was incubated at room temperature for 15 min to allow binding between the compound and CYP24A1. All DNA components (if applicable) were heated at 95 °C for 5 min prior to use to facilitate three-dimensional conformation formation, immediately chilled on ice for 5 min, and then stored at room temperature until use. They were diluted in binding buffer when needed. Following the compound binding reaction, 5 μM 1,25-dihydroxyvitamin D_3 (1,25-D3, Cayman Chemical) and 1 mM NADPH were added to the system, followed by further incubation at 37 °C for 10 min. The metabolite conversion rate was analyzed using high-performance liquid chromatography (HPLC). CYP24-dependent reactions were terminated by adding a fourfold volume of chloroform/methanol (3 : 1, v/v). After vigorous vortexing, the organic phase was collected, dried, and

reconstituted in 100% acetonitrile. The solution was centrifuged at 20 000*g* for 15 min, and the supernatant was subjected to HPLC analysis under the following conditions: column, Capcell Pak C18 UG120 (4.6 mm inner diameter × 250 mm, 5 μm); UV detection wavelength, 265 nm; flow rate, 1 mL min^{-1}; column temperature, 40 °C; elution with a linear gradient of 20–100% acetonitrile in water over 25 min, followed by an additional 5-minute isocratic elution with 100% acetonitrile.[26]

4.12 Evaluation of the retention effect of compound 3c on $1,25(OH)_2D_3$

Three replicate culture wells ($N = 3$) were set up for each condition: a solvent control (0.2% v/v ethanol), a control with 10^{-7} M compound **3c** alone, a group treated with 5×10^{-10} M $1,25(OH)_2D_3$ alone, and two combination groups with this concentration of $1,25(OH)_2D_3$ plus 10^{-8} M or 10^{-7} M of compound **3c**, respectively. After treatment, the supernatant from each well was collected and stored at −80 °C together with the zero-time point samples for subsequent LC-MS/MS analysis of $1,25(OH)_2D_3$.

For the LC-MS/MS analysis, calibrators were prepared in phosphate-buffered saline (PBS), and all samples were appropriately diluted with PBS to fall within the linear range of the assay. The LC-MS/MS method was adapted from a previous protocol with modifications to enhance sensitivity: the initial sample volume was increased to 200 μL (instead of 50 μL), and after derivatization, the final derivatized $1,25(OH)_2D_3$ was reconstituted in 20 μL, with 15 μL injected (compared to the original method of reconstitution in 25 μL and injection of 5 μL). Based on a previous study, quantification was performed using multiple reaction monitoring (MRM) for the $1,25(OH)_2D_3$-DAPTAD derivative and its deuterated isotopic analog ($1,25(OH)_2D_3$-d_6).[27]

4.13 Statistical analysis

The above experimental data is the average ± SEM (standard error of mean) for at least three data points from independent experiments. SPSS 21.0 software was used to analyze the data, and one-way analysis of variance (ANOVA) was used to process the statistical differences between the two groups.

Conflicts of interest

The authors declare that the research was conducted in the absence of any commercial or financial relationships that could be construed as a potential conflict of interest.

Data availability

Data will be made available on request.

Supplementary information is available. See DOI: https://doi.org/10.1039/d5ra06803g.

References

1 P. Punzón-Jiménez and E. Labarta, The impact of the female genital tract microbiome in women health and reproduction: a review, *J. Assist. Reprod. Genet.*, 2021, **38**, 2519–2541, DOI: 10.1007/s10815-021-02247-5.
2 J. Fróes, T. S. Toma, M. Jachiet, L. Rousset, R. E. Poderoso and M. A. B. Trindade, Bacterial, fungal and parasitic co-infections in leprosy: A scoping review, *PLoS Neglected Trop. Dis.*, 2023, **17**, 0011334, DOI: 10.1371/journal.pntd.0011334.
3 G. Wei, Q. Liu, X. Wang, Z. Zhou, X. Zhao, W. Zhou, W. Liu, Y. Zhang, S. Liu, C. Zhu and H. Wei, A probiotic nanozyme hydrogel regulates vaginal microenvironment for *Candida* vaginitis therapy, *Sci. Adv.*, 2023, **9**, 0949, DOI: 10.1126/sciadv.adg0949.
4 P. Liu, Y. Lu, R. Li and X. Chen, Use of probiotic lactobacilli in the treatment of vaginal infections: *In vitro* and *in vivo* investigations, *Front. Cell. Infect. Microbiol.*, 2023, **13**, 1153894, DOI: 10.3389/fcimb.2023.1153894.
5 V. C. Kalia, S. K. S. Patel and J. K. Lee, Bacterial biofilm inhibitors: An overview, *Ecotoxicol. Environ. Saf.*, 2023, **264**, 115389, DOI: 10.1016/j.ecoenv.2023.115389.
6 G. Suleyman and G. J. Alangaden, Nosocomial Fungal Infections: Epidemiology, Infection Control, and Prevention, *Infect. Dis. Clin. North Am.*, 2021, **35**, 1027–1053, DOI: 10.1016/j.idc.2021.08.002.
7 J. Beardsley, C. L. Halliday, S. C. Chen and T. C. Sorrell, Responding to the emergence of antifungal drug resistance: perspectives from the bench and the bedside, *Future Microbiol.*, 2018, **13**, 1175–1191, DOI: 10.2217/fmb-2018-0059.
8 P. Jangir, S. Kalra, S. Tanwar and V. K. Bari, Azole resistance in Candida auris: mechanisms and combinatorial therapy, *APMIS*, 2023, **131**, 442–462, DOI: 10.1111/apm.13336.
9 Q. Lu, T. C. A. Hitch, J. Y. Zhou, M. Dwidar, N. Sangwan, D. Lawrence, L. S. Nolan, S. T. Espenschied, K. P. Newhall, Y. Han, P. E. Karell, V. Salazar, M. T. Baldridge, T. Clavel and T. S. Stappenbeck, A host-adapted auxotrophic gut symbiont induces mucosal immunodeficiency, *Science*, 2024, **385**, 2536, DOI: 10.1126/science.adk2536.
10 Y. Belkaid and J. A. Segre, Dialogue between skin microbiota and immunity, *Science*, 2014, **346**, 954–959, DOI: 10.1126/science.1260144.
11 A. R. Han, S. Lee, J. Cha, J. Y. Kim, D. K. Kim, J. W. Han, C. J. Kim and S. K. Lee, Genital tract infection and pelvic surgery contribute to the development of endometriosis, *J. Reprod. Immunol.*, 2023, **156**, 103831, DOI: 10.1016/j.jri.2023.103831.
12 M. A. Maestro, F. Molnár and C. Carlberg, Vitamin D and Its Synthetic Analogs, *J. Med. Chem.*, 2019, **62**, 6854–6875, DOI: 10.1021/acs.jmedchem.9b00208.
13 C. Wang, B. Wang, L. Xue, Z. Kang, S. Hou, J. Du and C. Zhang, Design, Synthesis, and Antifibrosis Activity in Liver of Nonsecosteroidal Vitamin D Receptor Agonists

with Phenyl-pyrrolyl Pentane Skeleton, *J. Med. Chem.*, 2018, **61**, 10573–10587, DOI: 10.1021/acs.jmedchem.8b01165.

14 R. Otero, M. Ishizawa, N. Numoto, T. Ikura, N. Ito, H. Tokiwa, A. Mouriño, M. Makishima and S. Yamada, 25S-Adamantyl-23-yne-26,27-dinor-1α,25-dihydroxyvitamin D3: Synthesis, Tissue Selective Biological Activities, and X-ray Crystal Structural Analysis of Its Vitamin D Receptor Complex, *J. Med. Chem.*, 2018, **61**, 6658–6673, DOI: 10.1021/acs.jmedchem.8b00427.

15 F. Sarmadi, Z. Gao, J. Su, C. Barbier, P. Artusa, K. Bijian, J. L. Gleason and J. H. White, Bifunctionality and Antitumor Efficacy of ZG-126, a Vitamin D Receptor Agonist/Histone Deacetylase Inhibitor Hybrid Molecule, *J. Med. Chem.*, 2024, **67**, 11182–11196, DOI: 10.1021/acs.jmedchem.4c00706.

16 C. Carlberg and A. Muñoz, An update on vitamin D signaling and cancer, *Semin. Cancer Biol.*, 2022, **79**, 217–230, DOI: 10.1016/j.semcancer.2020.05.018.

17 D. W. Denning, Global incidence and mortality of severe fungal disease, *Lancet Infect. Dis.*, 2024, **24**, 428–438, DOI: 10.1016/S1473-3099(23)00692-8.

18 Y. Su, G. Ganguli-Indra, N. Bhattacharya, I. E. Logan, A. K. Indra, A. F. Gombart, S. L. Wong and J. Xie, Codelivery of 1α,25-Dihydroxyvitamin D3 and CYP24A1 Inhibitor VID400 by Nanofiber Dressings Promotes Endogenous Antimicrobial Peptide LL-37 Induction, *Mol. Pharm.*, 2022, **19**, 974–984, DOI: 10.1021/acs.molpharmaceut.1c00944.

19 L. Emami, Z. Faghih, E. Ataollahi, S. Sadeghian, Z. Rezaei and S. Khabnadideh, Azole Derivatives: Recent Advances as Potent Antibacterial and Antifungal Agents, *Curr. Med. Chem.*, 2023, **30**, 220–249, DOI: 10.2174/0929867329666220407094430.

20 S. Hong, H. Lu, D. Tian, Y. Chang, Q. Lu and F. Gao, Discovery of triazole derivatives for biofilm disruption, anti-inflammation and metal ion chelation, *Front. Chem.*, 2025, **26**, 1545259, DOI: 10.3389/fchem.2025.1545259.

21 B. Koodziej, M. Morawiak and W. Schilf, Structure investigations of Schiff bases derived from 3-amino-1H-1,2,4-triazole, *J. Mol. Struct.*, 2019, **1184**, 12, DOI: 10.1016/j.molstruc.2019.02.027.

22 L. Li, H. Wu, J. Wang, Z. Ji, T. Fang, H. Lu, L. Yan, F. Shen, D. Zhang, Y. Jiang and T. Ni, Discovery of Novel 8-Hydroxyquinoline Derivatives with Potent *In Vitro* and *In Vivo* Antifungal Activity, *J. Med. Chem.*, 2023, **66**, 16364–16376, DOI: 10.1021/acs.jmedchem.3c01771.

23 R. Elias, P. Basu and M. Fridman, Fluconazole-COX Inhibitor Hybrids: A Dual-Acting Class of Antifungal Azoles, *J. Med. Chem.*, 2022, **65**, 2361–2373, DOI: 10.1021/acs.jmedchem.1c01807.

24 I. P. Sæbø, M. Bjørås, H. Franzyk, E. Helgesen and J. A. Booth, Optimization of the Hemolysis Assay for the Assessment of Cytotoxicity, *Int. J. Mol. Sci.*, 2023, **24**, 2914, DOI: 10.3390/ijms24032914.

25 S. Lin, W. L. W. Sin, J. J. Koh, F. Lim, L. Wang, D. Cao, R. W. Beuerman, L. Ren and S. Liu, Semisynthesis and Biological Evaluation of Xanthone Amphiphilics as Selective, Highly Potent Antifungal Agents to Combat Fungal Resistance, *J. Med. Chem.*, 2017, **60**, 10135–10150, DOI: 10.1021/acs.jmedchem.

26 M. Biyani, K. Yasuda, Y. Isogai, Y. Okamoto, W. Weilin, N. Kodera, H. Flechsig, T. Sakaki, M. Nakajima and M. Biyani, Novel DNA Aptamer for CYP24A1 Inhibition with Enhanced Antiproliferative Activity in Cancer Cells, *ACS Appl. Mater. Interfaces*, 2022, **14**, 18064–18078, DOI: 10.1021/acsami.1c22965.

27 A. K. Alshabrawy, Y. Cui, C. Sylvester, D. Yang, E. S. Petito, K. R. Barratt, R. K. Sawyer, J. K. Heatlie, R. Polara, M. J. Sykes, G. J. Atkins, S. M. Hickey, M. D. Wiese, A. M. Stringer, Z. Liu and P. H. Anderson, Therapeutic Potential of a Novel Vitamin D3 Oxime Analogue, VD1-6, with CYP24A1 Enzyme Inhibitory Activity and Negligible Vitamin D Receptor Binding, *Biomolecules*, 2022, **12**, 960, DOI: 10.3390/biom12070960.

28 Z. Li, L. Zhao, Y. Bian, Y. Li, J. Qu and F. Song, The Antibacterial Activity of Quinazoline and Quinazolinone Hybrids, *Curr. Top. Med. Chem.*, 2022, **22**, 1035–1044, DOI: 10.2174/1568026622666220307144015.

29 Q. Wu, Z. Yang, Y. Nie, Y. Shi and D. Fan, Multi-drug resistance in cancer chemotherapeutics: mechanisms and lab approaches, *Cancer Lett.*, 2014, **347**, 159–166, DOI: 10.1016/j.canlet.2014.03.013.

30 G. Milli, A. Pellegrini, R. Listro, M. Fasolini, K. Pagano, L. Ragona, G. Pietrocola, P. Linciano and S. Collina, New LsrK Ligands as AI-2 Quorum Sensing Interfering Compounds against Biofilm Formation, *J. Med. Chem.*, 2024, **67**, 18139–18156, DOI: 10.1021/acs.jmedchem.